Effects of anatase TiO_2 morphology and surface fluorination on environmentally relevant photocatalytic reduction and oxidation reactions

M. V. Dozzi[a,*], M. Montalbano[a], G. Marra[b], L. Mino,[c] E. Selli[a]

[a] *Dipartimento di Chimica, Università degli Studi di Milano, via C. Golgi 19, I-20133 Milano, Italy*

[b] *Eni S.p.A Renewable Energy, Magnetic Fusion and Material Science Research Center (DE-R&D), via G. Fauser 4, I-28100 Novara, Italy*

[c] *Dipartimento di Chimica and NIS Centre, University of Torino, via P. Giuria 7, I-10125 Torino, Italy*

A B S T R A C T

Aiming at clarifying the interplay on TiO_2 photoactivity between particle morphology and surface fluorination, the photocatalytic performance of anatase nanocrystals, characterized by a pseudo-spherical shape or a nanosheet structure, is investigated in both a reduction and an oxidation reaction, either in the absence or in the presence of added fluoride anions. Cr(VI) photocatalytic reduction is strongly favored by a large exposure of anatase {001} facets, but surface fluorination leads in this case to a morphology-independent photoactivity decrease, due to the decreased adsorption of the reaction substrate. More interestingly, a beneficial synergistic effect between the platelet-like anatase morphology and TiO_2 surface fluorination is clearly outlined in Rhodamine B photocatalytic degradation, possibly resulting from the intrinsic ability of fluorinated {001} anatase facets of boosting $^{\bullet}OH$ radical mediated oxidation paths, due to their larger amount of surface −OH groups, as revealed by FT-IR spectroscopy.

Keywords: platelet-like TiO_2, {001} facets, surface fluorination, Cr(VI) photocatalytic reduction, Rhodamine B photocatalytic degradation

* Corresponding author.
E-mail address: mariavittoria.dozzi@unimi.it (M.V. Dozzi).

1. INTRODUCTION

The design and synthesis of cost effective, efficient and scalable TiO_2-based materials able to convert light into chemical energy through photocatalytic processes is a key challenge for a sustainable energy economy. A wide variety of synthetic routes has been developed to prepare TiO_2 in different forms and shapes, with different surface area and porosity [1–3], and to improve its photocatalytic activity, either by enhancing light absorption [4–7] or by improving the separation of photoproduced charge couples [8–11].

In particular, shape-controlled anatase TiO_2 has been prepared mainly by adding capping agents during the synthesis, which may preferentially stabilize the {001} facets during the crystal growth, with the production of nanocrystals with a platelet-like shape (see Scheme 1) [12–15]. The {001} facets, though thermodynamically less stable, are expected to be more reactive than the dominant {101} ones, mainly due to a high density and a very strained configuration of surface undercoordinated Ti atoms. Moreover, by tailoring the truncation degree of anatase crystals, the overall photoactivity may be further increased as a direct consequence of the selective migration of photogenerated holes towards the {001} facets and of photopromoted electrons to the {101} facets [16].

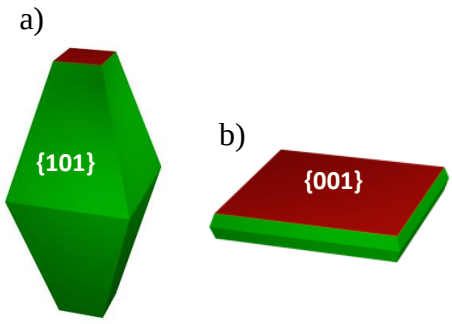

Scheme 1. (a) Equilibrium crystal shape and (b) platelet-like morphology of anatase crystals with the indication of the type of main exposed facets.

Fluoride anions are often used as capping agents in the synthesis of shape controlled anatase [17–23] and the effects on photoactivity of residual surface fluorination are very difficult to be disentangled from those deriving from the morphology of the material. Indeed, platelet-like anatase is usually synthesized in the presence of a higher fluoride ion concentration than spherically shaped TiO_2 [14,16,24]. The different amount of residual adsorbed fluoride anions for these two morphologies prevents one to appreciate the existence of synergistic effects between surface fluorination and morphology control in boosting the photoactivity of TiO_2-based materials [16].

In fact, surface fluorination, implying the following simple ligand exchange reaction between fluoride anions and surface hydroxyl groups (at acidic pH)

$$\equiv \mathrm{Ti} - \mathrm{OH} + \mathrm{F}^- \rightarrow \equiv \mathrm{Ti} - \mathrm{F} + \mathrm{OH}^- \qquad (1)$$

may induce different effects on photocatalysis, depending not only on the main degradation paths of different substrates [25], but also on the surface area and phase composition of TiO_2 [26], and may definitely improve the photocatalytic performance of TiO_2 [27–30].

In the present work we investigate the effects that TiO_2 surface fluorination has on photocatalytic oxidation and reduction reactions in relation to the amount of exposed anatase {001} facets. Fluorine-free TiO_2 materials with different morphology were obtained through a post-synthesis washing procedure that efficiently removed the capping agent. Such materials were then eventually *in-situ* re-fluorinated. Bare and re-fluorinated home-made photocatalysts were systematically tested in both Cr(VI) reduction and Rhodamine B photobleaching, which proceed through completely different mechanistic routes [31–33].

These two test reactions are important applications of photocatalysis as an environmentally friendly technology for industrial wastewaters decontamination [34–39]. In fact, hexavalent Cr(VI) ions, notoriously toxic and carcinogenic [40] and generally released in effluents by various industrial activities (*e.g.* electroplating, leather tanning, textile production, steel

fabrication), can be efficiently converted by photocatalytic reduction on semiconductors into Cr(III) species, exhibiting lower toxicity and mobility in the environment [41]. At the same time, the demand for Rhodamine B (RhB) conversion into harmless chemicals has also started growing in the recent years for a sustainable recycling of industrial wastewaters, due to the increased use of xanthene-derived dyes in food, paper, textile and leather industry. The undesired presence of RhB (see Scheme 2) in waters and food represents a serious threat for the human health due to its ability of causing injury to human skin, eyes, respiratory system, besides being potentially carcinogenic and neurotoxic [42,43].

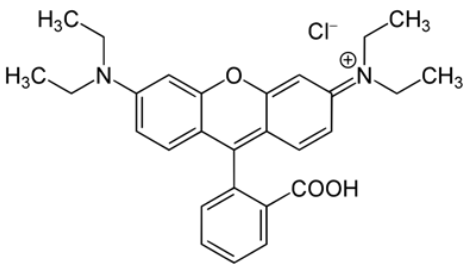

Scheme 2. Rhodamine B (RhB)

2. EXPERIMENTAL SECTION

2.1. Photocatalysts preparation

Differently shaped TiO_2 samples, characterized by a pseudo-spherical shape or a nanosheet structure, were prepared through the hydrothermal route by employing titanium isopropoxide as Ti precursor and HF as capping agent [24,44]. A fixed amount of titanium isopropoxide (10 mL) was mixed with 0.12 or 1.20 mL of a 48 wt% HF solution under stirring for 15 min in a Teflon liner. Water was also added in the first case in order to gain a 11.2 mL final volume in both cases. A reference sample was prepared under the same conditions by simply adding 1.2 mL of water (and no HF) to titanium isopropoxide.

The liner was then inserted into a closed stainless-steel autoclave and heated at 180 °C for 24 h. The obtained precipitate was recovered after cooling the autoclave down to room temperature using a stream of compressed air. A series of washing cycles with ultrapure Milli-Q water followed, up to a fluoride ion concentration in the supernatant, detected by means of ionic chromatography (Methrohm 761 compact IC with conductivity detector), below 5 ppm. The solid was then collected, dried in an electric oven at 70 °C overnight, and ground into a fine powder in an agate mortar. The so-obtained materials were labelled as HT_X, where HT refers to the adopted hydrothermal preparation method and X stands for the nominal F/Ti ratio employed during the synthesis, *i.e.* 0.1 or 1.0. The reference sample was labelled as HT_0, as no HF was used during its synthesis.

In order to remove the residual fluorine on the materials' surface, a portion of each sample underwent washing cycles with a 0.1 M NaOH aqueous solution. A fixed amount of photocatalyst (1.0 g) was dispersed in 200 mL of the NaOH solution by means of a 30 min ultrasonic treatment. The suspension was then left stirring in the dark for 1 h at 60 °C, followed by a 10 h-long stirring in the dark at room temperature [45]. The powders were then recovered by centrifugation and washed up to six times with Milli-Q water (200 mL) until a neutral pH was reached, and finally dried at 70 °C overnight. The so-obtained washed samples were labelled as HT_X_NaOH.

All reagents were purchased from Sigma-Aldrich and employed as received. Water purified by a Milli-Q water system (Millipore) was used throughout.

2.2. Photocatalysts characterization

X-Ray Powder Diffraction (XRPD) patterns were acquired using a Panalytical X'Pert Pro diffractometer, using Ni-Filtered Cu K_α radiation (λ=1.54056 Å) at a scan rate of 0.05 deg s^{-1}. The phase composition and the relative amount of exposed {001} facets of the investigated

samples were calculated by applying a Rietveld-based approach on diffraction data [46] using the GSAS-II software [47].

The specific surface area (SSA) of the samples was obtained by measuring N_2 adsorption/desorption isotherms at liquid nitrogen temperature according to the Brunauer-Emmet-Teller (BET) method employing a Micrometrics Tristar II 3020 V1.03 apparatus equipped with an ASAP 2020 surface area and porosity analyzer, after outgassing at 150 °C for 2 h under constant nitrogen flux. SSA data were calculated by the instrument provided software starting from the linear region of the BET isotherm, using the linearized form of the BET equation.

The UV-visible absorption spectra of the materials in powder form were acquired in diffuse reflectance (DR) mode using a Jasco V-670 spectrophotometer equipped with a PIN-757 integrating sphere, using barium sulfate as a reference standard. Reflectance (R) spectra in the 200-800 nm region, with a 1 nm spectral resolution, were converted into absorption (A) spectra using the relation $A = 1 – R$.

HRTEM analysis was carried out with a JEOL JEM 2010 electron microscope, equipped with a LAB6 electron gun operating at 200 keV and a Gatan CCD camera allowing high-resolution imaging. Specimens for HRTEM analysis were sonicated in 2-propanol and then transferred as a suspension to a copper grid covered with a holey carbon film. Micrographs were taken after solvent evaporation, spanning over the whole region of the sample, to achieve a truly representative statistical mapping of the investigated materials.

Thermogravimetric analysis (TGA) was carried out on a Mettler-Toledo TGA/DSC 2 STARe system. Thermograms were recorded in the 30-800 °C temperature range, with a heating ramp of 10 °C min^{-1} under a 50 cm^3 min^{-1} air flux.

X-Ray photoemission spectra (XPS) were recorded on a M-Probe apparatus, Surface Science Instruments, equipped with an Al-K_α monochromatic radiation X-Ray source (1486.6

eV photon energy). XPS surveys were recorded in a binding energy range from 1000 to 0 eV and peak shift correction was applied using the adventitious carbon C1s signal at 284.6 eV as internal reference.

For Fourier-transform infrared (FT-IR) spectroscopy measurements the samples were pressed in self-supporting pellets ("optical density" of ca. 10 mg cm^{-2}) and placed in quartz cells equipped with KBr windows designed to carry out spectroscopic analysis in controlled atmosphere. The thermal treatments at increasing temperatures (150, 300 and 500 °C) were performed for 90 min under dynamic vacuum (residual pressure < 1×10^{-4} mbar). At the end of each treatment step, the samples were contacted with O_2 at 10 mbar to restore the stoichiometry of TiO_2. The spectra were obtained using a Bruker Equinox 55 spectrometer with a 2 cm^{-1} resolution and by averaging 64 scans. The optical density of the pellets was employed to normalize all acquired spectra.

2.3. Photocatalytic activity tests

The photocatalytic activity of home-made samples was tested in aqueous suspensions, employing dichromate ($Cr_2O_7^{2-}$) ions or the dye Rhodamine B (RhB) as inorganic or organic degradation substrates, respectively. The photostability of both substrates in aqueous solution was preliminarily verified under the adopted irradiation conditions.

All photocatalytic degradation runs were performed under atmospheric conditions using the already described 100 ml photoreactor and setup [48]. In particular, the irradiation source was an Osram Powerstar HCI-T 150 W lamp, emitting at $\lambda > 340$ nm with an average full emission intensity on the reactor of *ca.* 110 mW cm^{-2}, as regularly checked with a Thorlabs PM200 optical power meter equipped with a thermal Thorlabs S302C power sensor. The whole set up was maintained at ambient temperature by a continuous stream of air.

In all kinetic runs, the TiO_2 content of the irradiated aqueous suspensions was 0.1 g L^{-1}. Aqueous TiO_2 suspensions were preliminary treated with ultrasound for 30 min in order to

ensure the de-aggregation of the photocatalyst particles, prior to the addition of an aqueous solution containing the inorganic or organic substrate. So-called natural pH conditions were obtained by this way. When required, the pH was adjusted down to *ca.* 3.7 by adding small amounts of a concentrated $HClO_4$ aqueous solution, which was chosen thanks to the low affinity of ClO_4^- anions for TiO_2 [49]. In all Cr(VI) photocatalytic reduction runs the initial pH of the suspensions was fixed at pH 3.7. At this pH the reduction potential of the Cr(VI)/Cr(III) couple is more positive than the TiO_2 conduction band edge [50].

In-situ surface fluorination of the photocatalyst was attained by adding fluoride ions to the suspensions in the form of NaF, prior to the addition of the degradation substrates [25]. The overall fluoride concentration was fixed so as the F/Ti molar ratio in the aqueous suspension was 0.1 and 2 for Cr(VI) photoreduction and Rhodamine B photodegradation, respectively.

Then appropriate volumes of stock solutions containing Cr(VI) or RhB were added to fix the initial concentration of the photocatalytic reaction substrates in the aqueous suspensions at 3.3×10^{-5} M for Cr(VI), from a solution obtained by dissolving $K_2Cr_2O_7$ in water, and 1.0×10^{-5} M for RhB. Before starting irradiation, the so obtained suspensions were magnetically stirred in the dark for 15 min to attain the adsorption equilibrium of the substrates on the photocatalyst surface.

Stirring was continued during the runs. The lamp was always switched on at least 30 min before the beginning of irradiation. At different time intervals during the runs, 5 mL of the suspension were withdrawn from the reactor and centrifuged employing an EBA-20 Hettich centrifuge. The supernatant was analyzed colorimetrically for Cr(VI) residual content, using the 1,5-diphenylcarbazide method [51]. RhB photobleaching was monitored during the runs by spectrophotometric analysis at 553 nm, the maximum of RhB absorption. According to calibration the molar extinction coefficient of the dye at this wavelength is $\varepsilon = (9.92 \pm 0.02) \times$

10^4 M^{-1} cm^{-1}. All kinetic runs were performed up to *ca.* 70% substrate removal and repeated at least twice, to check their reproducibility.

2.4. Substrates adsorption measurements on TiO_2 and fluorinated TiO_2

The substrates affinity for the different photocatalysts were investigated by performing adsorption tests at pH 3.7, both in the presence and in the absence of NaF, under the same experimental conditions adopted during the photocatalytic runs, apart from the photocatalysts content, which was fixed at 1.0 g L^{-1}. The suspensions were kept under stirring in the dark and samples were withdrawn after 15, 60 and 180 min, centrifuged and analyzed to determine the Cr(VI) or RhB residual amount in the supernatant. Adsorption equilibrium was attained in 15-30 min, but adsorption data after 3 h-long equilibration were considered more reliable, as in previous studies [52].

3. RESULTS AND DISCUSSION

3.1. Photocatalysts characterization

XRPD diffractograms of all samples of the HT_X series were recorded to determine both the phase composition and the morphology of the materials. As shown in Fig. 1, all diffraction patterns perfectly match those of pure anatase.

Quantitative phase analysis, performed through Rietveld refinement with two additional parameters to describe the crystallite sizes anisotropy [46,53], exclude the presence of rutile, brookite or other phases such as $TiOF_2$ and indicate that all samples are composed of pure anatase independently of the amount of fluorine employed during their synthesis. With increasing fluorine content the width of reflections with (l>h,k) broadened, accompanied by shrinking of the peaks characterized by a strong h component, in the 35-50° 2θ range, indicating a change in crystal growth along specific crystallographic directions [24].

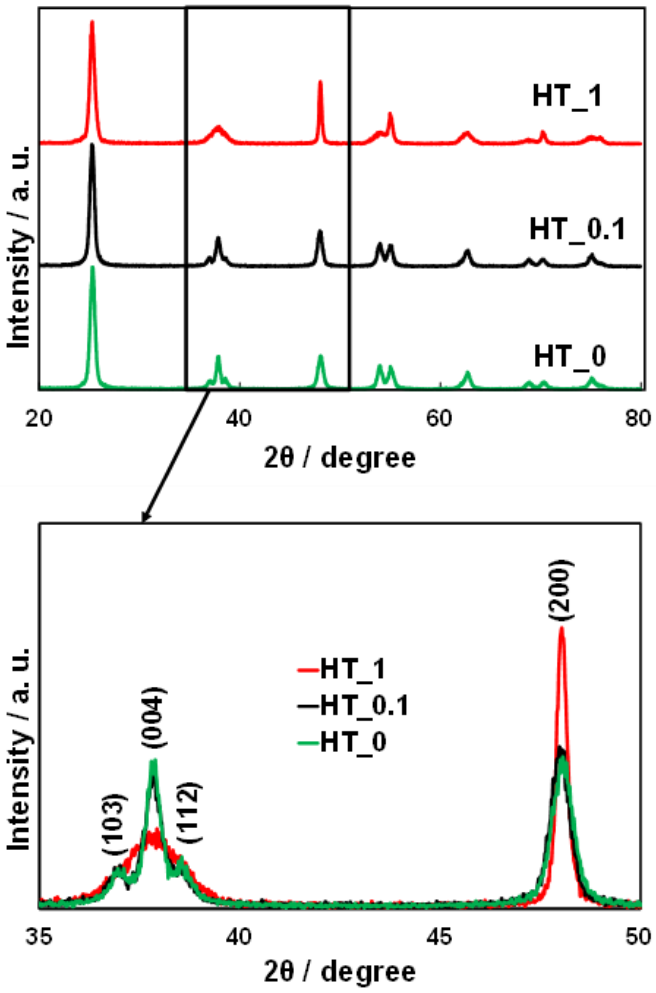

Fig. 1. XRPD patterns of HT_0 (green), HT_0.1 (black) and HT_1 (red trace) evidencing the (103), (004), (112), and (200) anatase reflections.

The nanoparticles size and the relative amount of exposed {001} facets in the different samples were calculated by applying an already described Rietveld-based XRPD approach [46] and are collected in Table 1. The percent amount of anatase {001} facets increased with increasing HF amount employed in the synthesis, passing from *ca.* 15% for HT_0.1 to 65% for HT_1, which incontrovertibly consisted of platelet-like nanocrystals, as confirmed by the HR-TEM images shown in Fig. 2a,b. In line with previous findings [24], the platelet-like crystals of HT_1 appeared piled up face-to-face, one above the other (Fig. 2b), thus minimizing the total surface energy [23,54]. On the contrary, HT_0.1 showed a casual distribution of the particles aggregates, as expected for nanocrystals with an isotropic shape (Fig. 2a).

Table 1. Average nanoparticles thickness and width, percent amount of exposed {001} facets, BET specific surface area (SSA) and total weight loss detected by TGA analysis.

Sample	thickness (nm)	width (nm)	{001} facets (%)	SSA (m^2 g^{-1})	Total weight loss (%)
HT_0	21.4 ± 0.4	14.6 ± 0.2	7.2 ± 0.6	93 ± 1	4
HT_0.1	17.2 ± 0.3	16.8 ± 0.3	14.8 ± 0.8	78 ± 1	5
HT_1	7.8 ± 0.2	39.0 ± 1.0	67.0 ± 2.0	84 ± 4	6
HT_0.1_NaOH	18.5 ± 0.8	16.5 ± 0.7	14.0 ± 0.2	82 ± 2	5
HT_1_NaOH	8.2 ± 0.2	38.0 ± 1.0	65.0 ± 1.0	82 ± 7	5

At the same time, HR-TEM images further confirmed both the crystal thickness and width values of platelet-like HT_1 nanoparticles, calculated from XRPD data [46] and corresponding to *ca.* 8 and 40 nm, respectively, as reported in Table 1. The procedure of capping agent removal did not significantly alter the percent amount of exposed {001} facets in any of the investigated materials (Table 1), the specific TiO_2 crystal shape being entirely preserved after washing (see Fig. 2c-f).

BET analysis confirmed similar SSA values in the 82-93 m^2 g^{-1} range, for both HT_X and HT_X_NaOH series, no significant SSA variation being observed upon washing with the NaOH solution. Reference HT_0, synthesized in the absence of fluoride anions, had a slightly higher SSA (Table 1). Thus, the photocatalytic activity of the materials can be directly compared, all of them having almost the same SSA. Representative N_2 adsorption-desorption isotherms of HT_0, HT_0.1 and HT_1 can be found in our previous paper [24].

The absorption spectra of the investigated samples are characterized by a marked absorption onset at *ca.* 400 nm, typical of pure anatase (see Fig. 3), independent of the F/Ti ratio employed during the synthesis, *i.e.* of the relative amount of exposed crystal facets (see inset of Fig. 3). The anatase band gap has been reported to be red- [55–57], blue- [24,58] shifted or unmodified [59,60] with increasing {001} facets content. Also the washing procedure did not produce any absorption edge variation, thus resulting in an overall preservation of the original optical properties of the materials (see Fig. 3). Moreover, the absorption spectra did not evidence the

presence of residual carbonaceous impurities adsorbed on the materials surface, which would produce absorption in the visible region [61], in line with the low and pretty similar percent total mass losses recorded for all samples by thermogravimetric analysis (TGA) (see Table 1).

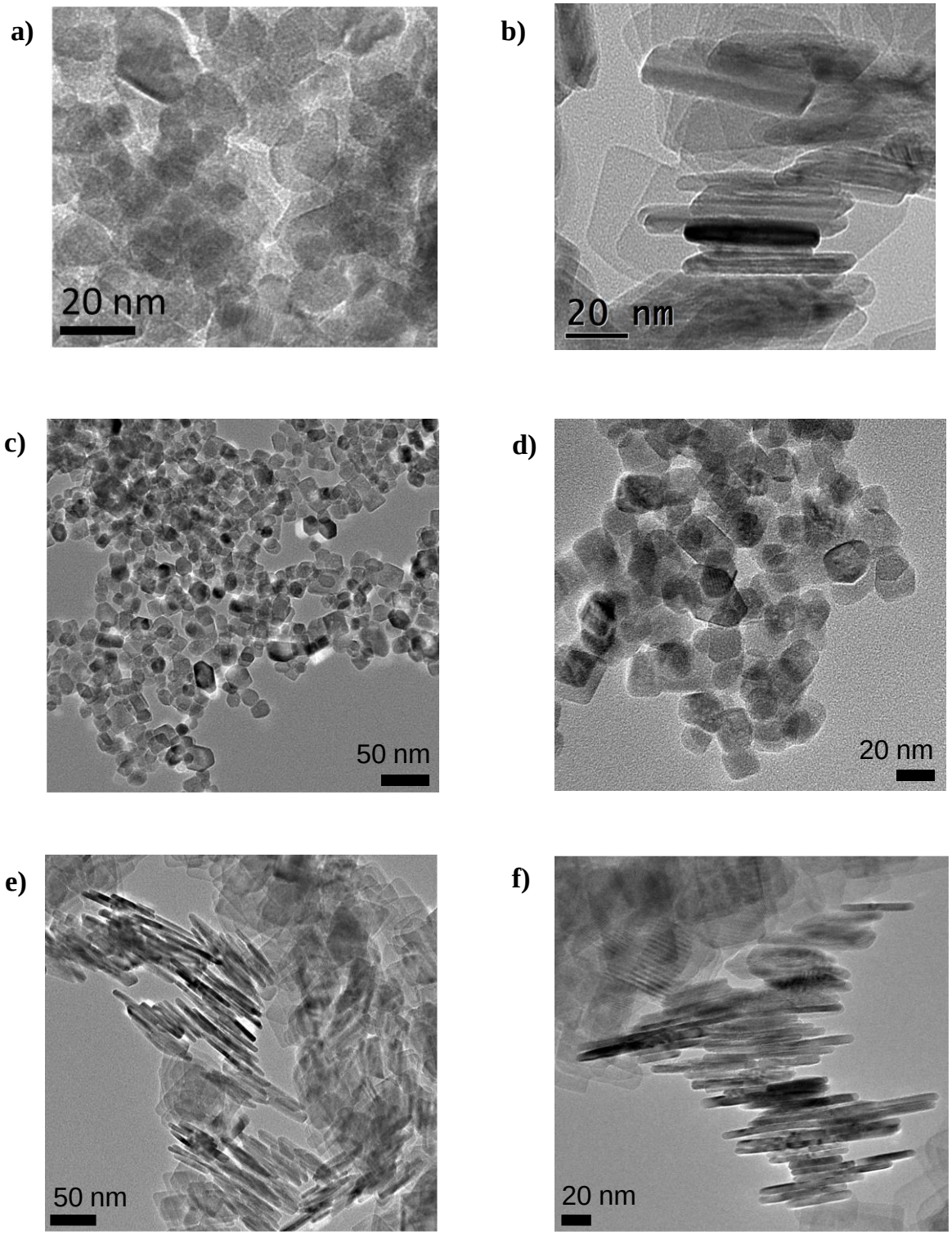

Fig. 2. HRTEM images of (a) HT_0.1, (b) HT_1, (c,d) HT_0.1_NaOH and (e,f) HT_1_NaOH.

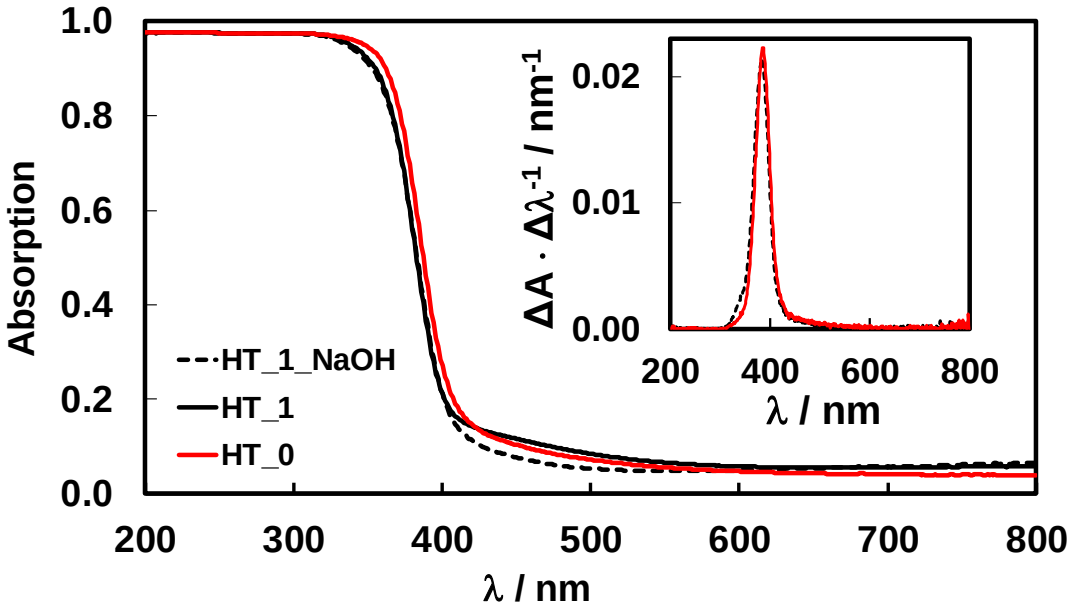

Fig. 3. Absorption spectra of HT_0 (red), HT_1 (black) and HT_1_NaOH (black dashed line). Inset: Numerical first derivative of the absorption spectra, highlighting invariance of the absorption band edge for different TiO_2 morphology.

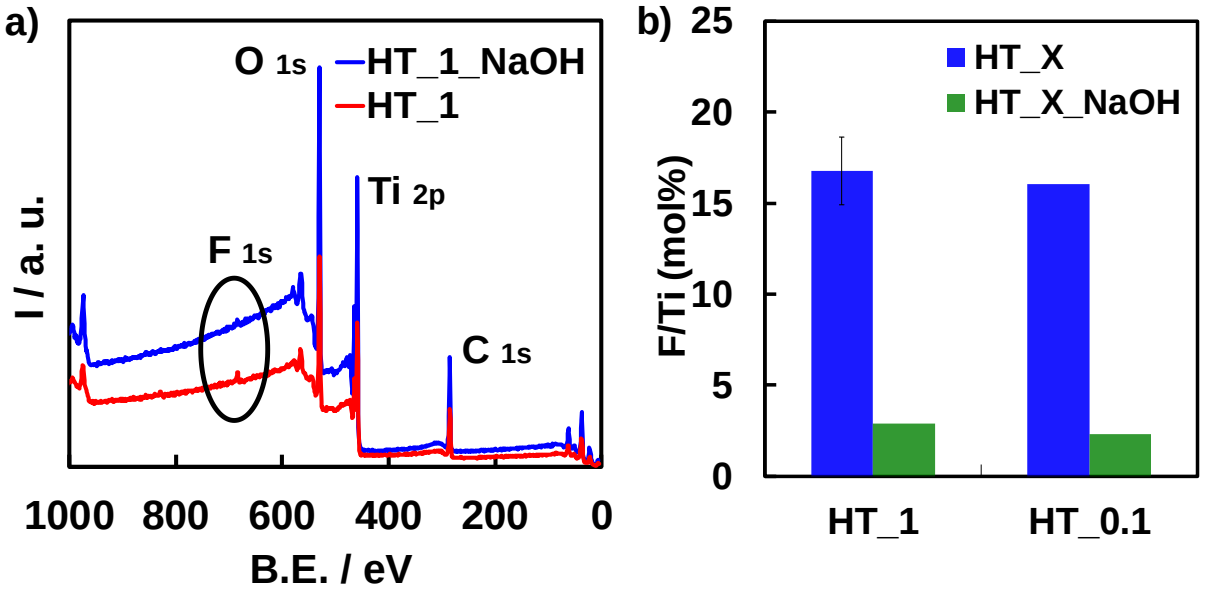

Fig. 4. (a) XPS survey spectra of HT_1 (red) and HT_1_NaOH (blue trace); the surface fluoride signal located at 684 eV is highlighted. (b) Surface F/Ti percent molar ratios in HT_X and HT_X_NaOH samples.

XPS analyses were performed in order to determine the surface chemical composition of the photocatalysts (Fig. 4). Titanium, carbon and oxygen were identified by the XPS signals at binding energies (BE) 458.8 eV (Ti 2p), 531 eV (O 1s) and 284.5 eV (C 1s), respectively. XPS

spectra of HT_1 and HT_0.1 also show a small peak at BE 684 eV attributed to F 1s [62,63], indicating the residual presence of fluoride anions on the surface of the synthesized materials. No XPS signal at 688 eV, assigned to substitutional F ions in the TiO_2 lattice, was detected, possibly always being below the detection limit of the XPS technique [24,64].

As shown in Fig. 4b, quantitative XPS analysis demonstrated the effective (though not complete) removal of the residual fluoride capping agent from HT_1 and HT_0.1 by the here applied post-synthesis washing procedure. In fact, the overall surface F/Ti ratios passed from *ca.* 0.16 to *ca.* 0.02 in both washed samples.

3.2. Cr(VI) adsorption and photocatalytic reduction

The effects induced on Cr(VI) adsorption on the investigated samples by the morphology of these latter and by their *in-situ* surface fluorination can be appreciated in Fig. 5, reporting the percent amounts of Cr(VI) adsorbed on both washed HT_0.1_NaOH and HT_1_NaOH at pH 3.7 and on the same photocatalysts after surface fluorination (equilibration with fluoride ions).

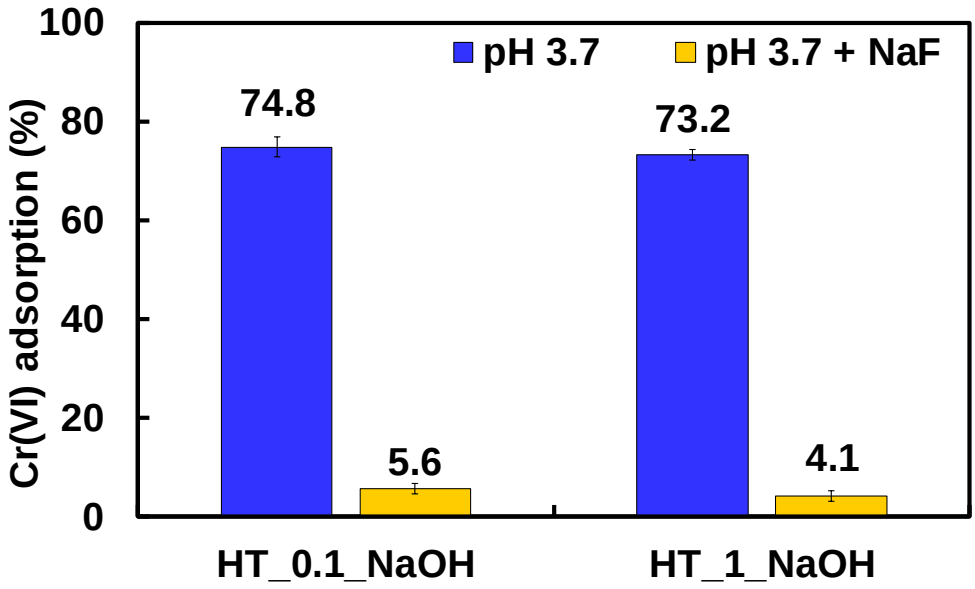

Fig. 5. Percent amount of Cr(VI) adsorbed onto HT_0.1_NaOH and HT_1_NaOH at pH 3.7 after 180 min stirring in the dark in the absence of fluoride ions (blue) and under *in-situ* fluorinated conditions, with a F/Ti ratio equal to 0.1 (yellow).

The adsorption of dichromate ions is strongly hampered upon surface fluorination of both differently shaped materials, even with the low fluoride amounts here employed (the F/Ti molar

ratio was only 0.1). Indeed, bare HT_0.1_NaOH and HT_1_NaOH are almost equally able to adsorb dichromate ions in the absence of light, independently of the extent of {001} facets exposure, and dichromate adsorption largely decreases to almost the same low value upon surface fluorination of both materials (Fig. 5).

In the absence of fluoride anions, the surface of titanium dioxide is rich in surface bound terminal $\equiv Ti-OH$ groups, which play a key role in ensuring dichromate adsorption on TiO_2 by means of surface complexation [65]. Moreover, at pH 3.7 the titanium dioxide surface is expected to be positively charged, this pH being below the point of zero charge (pH_{pzc}) of TiO_2, generally located at pH 5.6 [66]. These combined effects of course allow for a fast and significant adsorption of negatively charged $Cr_2O_7^{2-}$ anions on the TiO_2 bare surface [31,67]. Differently, *in-situ* fluorination implies the formation of stable $\equiv Ti-F$ terminations on the TiO_2 surface, with a consequent shift of the surface charge towards more negative values, in line with the location of the pH_{pzc} of fluorinated TiO_2 at *ca.* pH 4 [68], which hinders dichromate anions adsorption on the TiO_2 surface [69], as shown in Fig. 5.

In all photocatalytic runs, Cr(VI) concentration in the aqueous phase was found to decrease according to a first order rate law. Thus, the photocatalytic activity in this reaction of the here investigated materials can be compared in terms of first order rate constants, determined in aqueous suspensions at pH 3.7 either in the absence (k_{ac}) or in the presence of fluoride anions (*in-situ* fluorinated surface, k_F). These values are reported in Fig. 6.

Firstly, among HT_X_NaOH bare photocatalysts with different percent amounts of {001} facets, the platelet-like material is by far the best performing one, with an outstanding activity double to that of benchmark P25 TiO_2 (for which $k_{ac} = 3.3 \times 10^{-4}$ s^{-1} under identical experimental conditions). The k_{ac} value measured with HT_1_NaOH is also three-time larger than that obtained with HT_0.1_NaOH (Fig. 6). However, this outstanding photoactivity of the TiO_2 material with the higher percentage of exposed {001} facets cannot be explained in terms

of dichromate anions adsorption under dark conditions, which is very similar for platelet-like and spherical-shaped washed samples (Fig. 5). The observed photoactivity should result from multiple effects related to the anatase crystal morphology. In fact, a significant enhancement in photogenerated charge carrier separation may be attained with increasing {001} facets exposure in TiO_2, leading to platelet-like better performing materials [60,70–72].

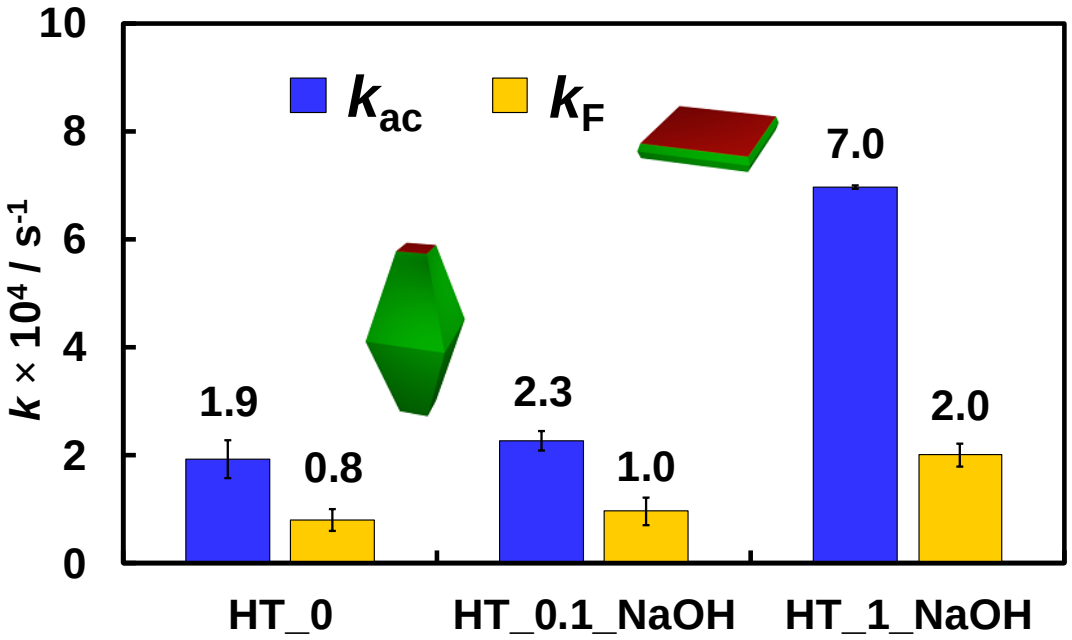

Fig. 6. First order rate constants of Cr(VI) photocatalytic reduction at pH 3.7 with bare (k_{ac}, in blue) and surface fluorinated (k_F, in yellow) photocatalysts.

Anatase crystals with different co-exposed facets can be envisaged forming 'surface heterojunctions' [60,70,73], with the selective migration of photogenerated holes and photopromoted electrons towards {001} and {101} facets, respectively, being driven by the minimization of their respective energies. In particular, an optimal percent mixture of different anatase facets may have positive effects in electron-hole pair separation, as in mixed anatase-rutile systems [74]. Of course, the optimal percent amount of exposed {001} facets in anatase materials, *i.e.* ensuring the highest photoactivity, depends on the relative rates of the two simultaneous (reduction and oxidation) semi-reactions involved in the overall investigated photocatalytic process, the best charge carrier separation being generally attained for anatase samples with *ca.* 50-60% {001} facets content. Interestingly, He *et al.* [17] reported a

maximum photoactivity in Cr(VI) reduction for TiO_2 materials showing a percent amount of {001} facets equal to 72%, which is comparable to the {001} facets exposure of the here investigated best performing HT_1_NaOH sample. This confirms that a balanced exposure of {001} and {101} facets is needed to achieve an optimal distribution of electrons and holes between them, possibly depending on the peculiar investigated substrate-sensitive process [60].

In addition, the overall efficiency of photocatalytic processes is generally affected by the extent and mode of substrate adsorption, which may also depend on the type of crystal facets predominantly exposed by the photocatalyst, since facets differ in their surface atomic structure [75,76].

In the specific case of Cr(VI) photocatalytic reduction, {001} facets, displaying 100% unsaturated surface Ti-5c and undercoordinated O-2c atoms, tend to favour the dissociative adsorption of water molecules, accompanied by the formation of terminal Ti−OH groups [77,78], possibly in a larger extent under irradiation conditions. Such TiO_2 surface bound −OH moieties may also behave as adsorption sites for fast and efficient dichromate anions adsorption [31,65], resulting in their faster conversion to Cr(III) through their direct interaction with electrons photopromoted in the TiO_2 conduction band [67]. However, by considering that the adsorption data collected in Fig. 5 do not evidence any remarkable difference in dichromate anions adsorption (at least under dark conditions) on the plate-like and the spherically-shaped sample, we expect that the presence of a relatively high amount of {001} facets may play a positive role in promoting the overall photocatalytic water oxidation semi-reaction on TiO_2, with consequent beneficial effects also on the simultaneous Cr(VI) photoreduction process.

Fig. 6 also shows that, regardless of the specific TiO_2 morphology, surface fluorination of washed samples leads to a conspicuous (*ca.* 60-70%) photoactivity decrease, most reasonably consequent to the dramatically reduced adsorption of negatively charged $Cr_2O_7^{2-}$ ions (Fig. 5). However, the extent of such photoactivity decrease is lower than the *ca*. 90% surface substrate

adsorption inhibition effect induced by *in-situ* fluorination (Fig. 5). Previous studies carried out by Ku *et al.* [31] also evidenced that the pH effects on Cr(VI) photocatalytic reduction rate were not correlated to Cr(VI) adsorption on the TiO_2 surface. Thus, Cr(VI) adsorption is not the only parameter directly influencing the rate determining step of Cr(VI) photoreduction, the overall photocatalytic process being also affected by photopromoted electrons transfer to adsorbed Cr(VI).

3.3. Rhodamine B adsorption and photocatalytic oxidation

Fig. 7 shows the results of RhB adsorption tests performed at pH 3.7 on the bare pseudo-spherical and platelet-like shaped materials (HT_0.1_NaOH and HT_1_NaOH, respectively) and on the same materials after surface fluorination. The adsorption of the cationic dye on TiO_2 at pH 3.7 is rather poor and further inhibited by *in-situ* TiO_2 fluorination, most likely due to alterations of the adsorption equilibrium upon substitution of $\equiv Ti-OH$ terminal groups with $\equiv Ti-F$ moieties, as for other organic dyes [69,79].

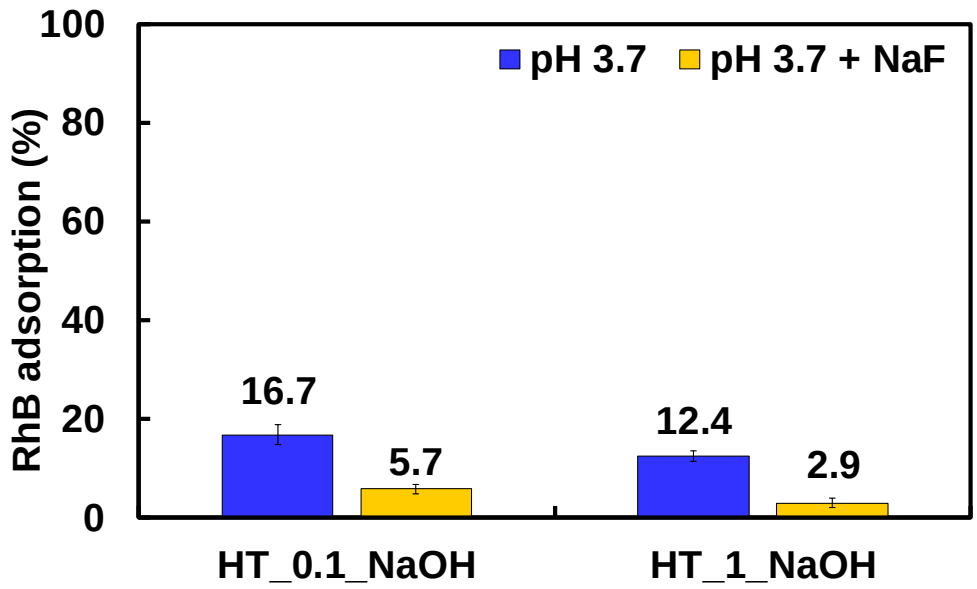

Fig. 7. Percent amount of RhB adsorbed on HT_0.1_NaOH and on HT_1_NaOH at pH 3.7 after 180 min stirring in the dark in the absence of fluoride ions (blue) and under *in-situ* fluorinated conditions, with a F/Ti ratio equal to 2 (yellow).

The adsorption of the organic substrate seems to be slightly hindered by a platelet-like TiO_2 morphology and this effect is maintained upon *in-situ* fluorination of the TiO_2 surface, the

percent amounts of adsorbed RhB decreasing by 76% and 66% upon HT_1_NaOH and HT_0.1_NaOH surface fluorination, respectively. This may indirectly suggest a more extensive {001} surface coverage with fluorinated sites, accompanied by a more marked RhB surface adsorption inhibition.

Firstly, in order to check that RhB photobleaching occurs through the photocatalytic path (and not through self-degradation), the photostability of Rhodamine B was confirmed by 6-hours long experiments at pH 3.7, both in the absence and in the presence of fluoride anions, under the here adopted UV-vis light irradiation. Furthermore, the absence of any RhB degradation during kinetic runs attained in the presence of photocatalyst employing a 420 nm cut off filter allowed us to exclude any dye-sensitized photocatalytic reaction path, which would be initiated by the selective dye excitation under visible light irradiation.

The photocatalytic degradation of RhB always occurred according to a first-order kinetics. The intensity of the RhB maximum absorption at 553 nm gradually decreased during the runs, with a very limited hypsochromic shift in the absorption maximum and no modification of the spectral shape (see Fig. 8a), which excludes the formation of large amounts of light absorbing intermediate species during the runs. Consequently, absorbance values at 553 nm can be taken as directly proportional to RhB residual concentration during the runs.

This supports the idea that the oxidative degradation of RhB mainly proceeds through the cleavage of the RhB chromophore group [32,80,81], which may occur via the direct interaction of RhB molecules with positive valence band holes (h_{VB}^{+}) photogenerated on the semiconductor surface or through an indirect, $^{\bullet}OH$ radical-mediated, degradation mechanism.

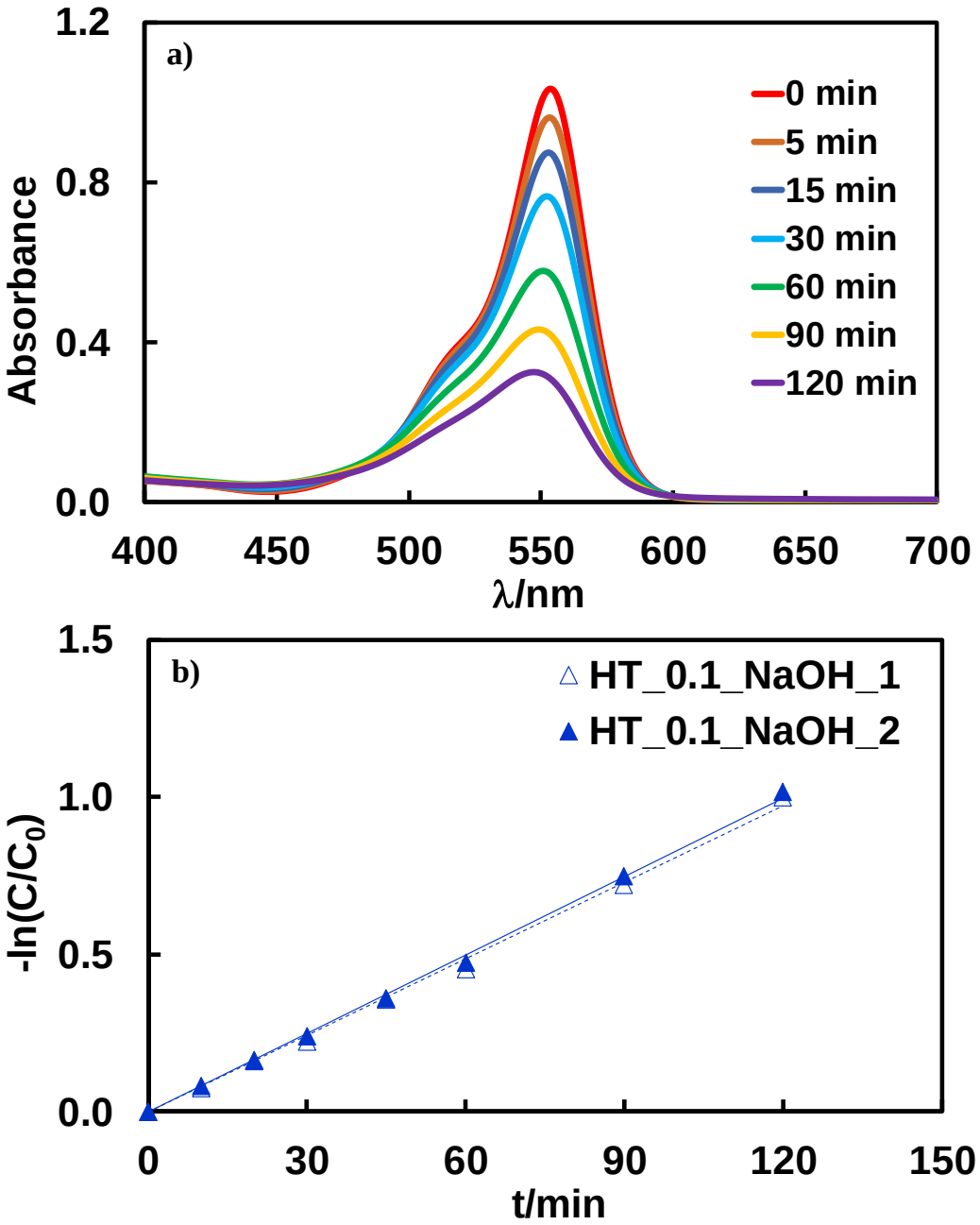

Fig. 8. (a) Absorption spectra recorded during RhB photocatalytic degradation in aqueous suspension at pH 3.7 with HT_0.1_NaOH; (b) data elaboration according to first order plots obtained in two runs under identical conditions (void and full triangles).

The photoactivity trend of the here investigated photocatalysts in RhB bleaching is shown in Fig. 9, which reports the first order rate constants of this reaction determined in aqueous suspensions at natural pH (k_{nat}), or at pH 3.7 in the absence (k_{ac}) or in the presence of fluoride ions (*in-situ* fluorinated surface, k_F).

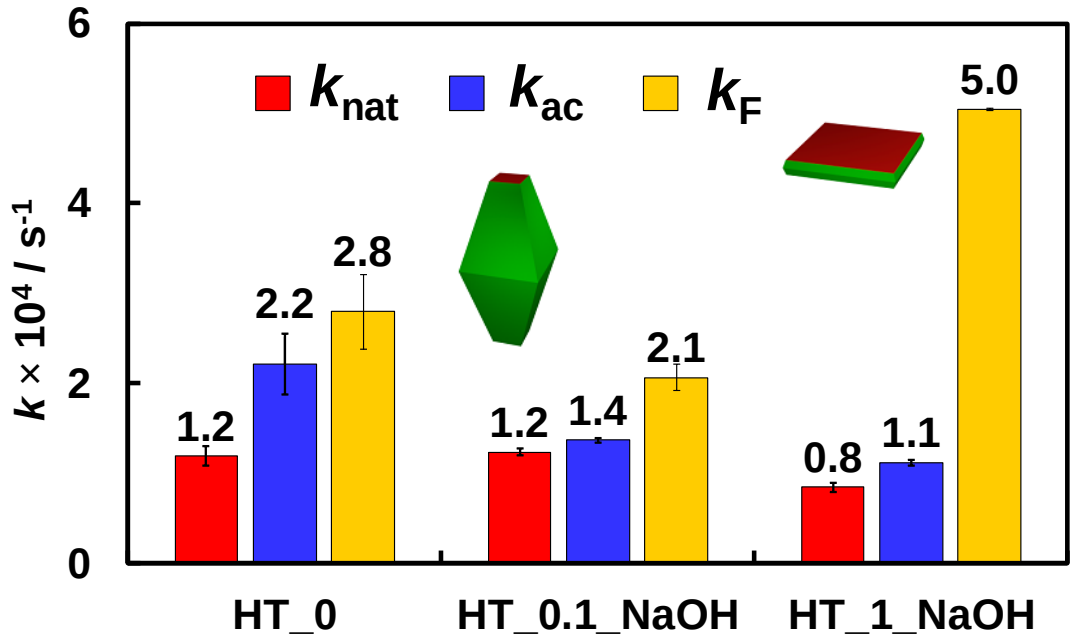

Fig. 9. First-order rate constants of RhB photocatalytic degradation with the investigated photocatalysts at natural pH (red, k_{nat}), at pH 3.7 in the absence of fluoride (blue, k_{ac}) or under *in-situ* fluorinated conditions, with a F/Ti ratio equal to 2 (yellow, k_F).

The photoactivity of the platelet-like material at natural pH or at pH 3.7 is quite similar to that of the anatase sample mainly exposing {101} facets. This indicates that the specific TiO_2 morphology does not significantly affect the rate of RhB photodegradation, at difference with respect to Cr(VI) photoreduction. Moreover, while lowering the pH has negligible effects on the reaction rate, surface TiO_2 fluorination, though hindering RhB adsorption, is beneficial for all materials.

Due to the relatively poor RhB adsorption on the photocatalysts surface, at difference with respect to Cr(VI) photoreduction, a direct reaction mechanism implying interaction between positive valence band holes (h_{VB}^+) photogenerated on the photocatalyst surface and adsorbed substrate molecules is not expected to be the main path of RhB photobleaching. The interaction of the dye molecules with hydroxyl radicals, formed upon h_{VB}^+-induced oxidation of water molecules, is expected to prevail in this case, and in particular with surface fluorinated TiO_2 materials, on which RhB adsorption is largely inhibited (Fig. 7).

In fact, an increase in RhB degradation rate upon TiO_2 surface fluorination can only be explained by considering an enhanced photoproduction of •OH radicals, which may attack RhB molecules and initiate their degradation [32,33,82]. Fluoride anions substituting for TiO_2 surface –OH groups inhibit surface trapping of photogenerated holes as ≡Ti-O• species, through the following reaction:

$$\equiv \mathrm{Ti} - \mathrm{OH} + \mathrm{h}_{vb}^{+} \rightarrow \equiv \mathrm{Ti} - \mathrm{O}^{\cdot} + \mathrm{H}^{+} \qquad (2)$$

At the same time, as $\equiv \mathrm{Ti} - \mathrm{F}$ species are stable and cannot be oxidized by valence band holes even at the here employed acidic pH [79], surface –F moieties favour the desorption of photogenerated active species, such as •OH radicals, which can thus accumulate in the aqueous phase [83], as follows:

$$\equiv \mathrm{Ti} - \mathrm{F} + \mathrm{h}_{vb}^{+} + \mathrm{H_2O} \rightarrow \equiv \mathrm{Ti} - \mathrm{F} + {}^{\cdot}\mathrm{OH} + \mathrm{H}^{+} \qquad (3)$$

An outstanding photoactivity increase was observed upon surface fluorination of {001}-facet enriched HT_1_NaOH, with a k_F/k_{ac} ratio of 4.52 (see Table 2), indicating a synergistic effect in RhB photocatalytic degradation between platelet-like anatase TiO_2 morphology and surface fluorination. Moreover, as reported in Table 2, similar k_F/k_{ac} ratios were obtained for both HT_1_NaOH and HT_1, which are significantly higher than the k_F/k_{ac} ratios obtained for HT_0.1_NaOH and HT_0.1. This confirms the here unveiled synergistic effect between platelet-like morphology and surface fluorination.

Moreover, the absence of any significant morphology-dependent RhB adsorption effect on fluorinated TiO_2 suggests that the increase of RhB photodegradation rate is related to the intrinsic ability of F-{001} facets of boosting •OH radical mediated oxidation paths, possibly due to an improved charge carriers separation, as previously reported by Chen *et al*. for the gas phase photocatalytic oxidation of ammonia [84]. The spontaneous tendency of photogenerated holes to migrate towards {001} facets [60,70,71] is amplified by the electric-field effect induced by surface fluorination [85], which increases holes attraction towards {001} facets

(present in larger extent) and photopromoted electrons repulsion from {001} facets, contributing in further conveying them towards {101} facets, with a consequent overall beneficial increase of photogenerated charge carriers separation.

Table 2. Ratios between the rate constants of RhB photocatalytic degradation performed with the investigated photocatalysts in aqueous suspensions at natural pH (k_{nat}), or at pH 3.7 in the absence (k_{ac}) or in the presence of fluoride ions (*in-situ* fluorinated surface, k_F).

Sample	k_{ac} / k_{nat}	k_F / k_{ac}
HT_0	1.86 ± 0.33	1.26 ± 0.27
HT_0.1_NaOH	1.11 ± 0.04	1.51 ± 0.11
HT_1_NaOH	1.33 ± 0.09	4.52 ± 0.15
HT_0.1	1.41 ± 0.10	1.42 ± 0.22
HT_1	1.22 ± 0.12	4.94 ± 0.02

At the same time the beneficial effect of surface fluorination on the photoactivity of platelet-like TiO_2 in RhB degradation may also originate from a larger initial exposure of surface −OH groups [77] (due to favored water molecules dissociation), leading to a higher surface density of fluorinated sites upon fluorination, which are involved in the production and release of reactive •OH radicals, as discussed above.

3.4. Amount of surface −OH groups by FT-IR analysis

A better insight at the molecular level into the differences in surface hydration and hydroxylation of HT_0.1_NaOH and HT_1_NaOH, was obtained by FT-IR spectroscopy. As shown in Fig. 10, reporting the FT-IR spectra recorded with these two photocatalysts after outgassing at different temperature, both samples at room temperature show a band at 1620 cm^{-1}, ascribed to $\delta(H_2O)$, the bending mode of adsorbed water [77]. Adsorbed H_2O molecules are not isolated, but are interacting by hydrogen bonding, as testified by the intense and broad ν(OH) band in the 3600-3000 cm^{-1} range [86].

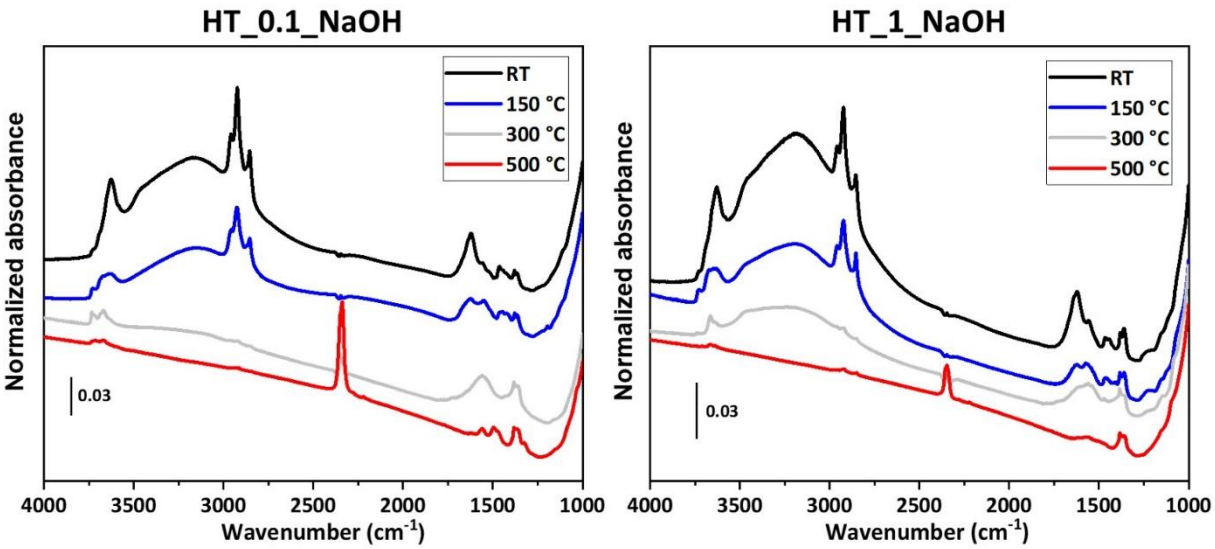

Fig. 10. FT-IR spectra of HT_0.1_NaOH (left) and HT_1_NaOH (right) outgassed for 1 h at room temperature (black), at 150 °C (blue), at 300 °C (grey) and at 500 °C (red trace).

In this spectral region also the IR signals of −OH groups are present, but they can be properly investigated only upon removing molecular water by outgassing at increasing temperatures. Heating at 150 °C considerably decreases the intensity of the $\delta(H_2O)$ band, which finally disappears at 300 °C, molecular water being completely removed from both samples by outgassing at such temperature. Considering the spectra recorded after outgassing at 300 °C (grey spectra in Fig. 10) in the ν(OH) spectral region, we note that HT_0.1_NaOH shows only some weak and sharp components at $\nu \geq 3600$ cm^{-1} due to few isolated −OH groups [78,87]. Conversely, HT_1_NaOH still exhibits a broad and quite intense band in the 3600-3000 cm^{-1} range, arising from a significant number of hydroxyl groups still present on {001} facets, which are expected to strongly adsorb water in a dissociative way [54,88]. Finally, outgassing at 500 °C nearly completely removes the −OH groups from both samples.

These FT-IR analysis results thus confirm that platelet-like TiO_2 presents a considerably higher concentration of surface −OH groups that can be converted into −F groups upon surface fluorination. This would favor the production, particularly on {001} facets, of hydroxyl

radicals, which are expected to be the main oxygen reactive species involved in the photocatalytic oxidation of RhB molecules.

4. CONCLUSIONS

In the present study we shed light on the combined effects of surface fluorination and morphology control in a reduction and an oxidation photocatalytic test reactions. Cr(VI) photoreduction is strongly favored by a larger exposure of {001} facets, with the best performing material having a platelet-like morphology, possibly due to improved charge separation arising from an optimal mixture of co-exposed facets, which favours the selective migration of photogenerated holes and electrons towards {001} and {101} facets, respectively. *In-situ* surface re-fluorination of the materials, however, leads to a morphology independent photoactivity decrease, consequent to the reduced ability of the fluorinated oxide to bind dichromate anions, a key step required for their direct reduction by conduction band electrons.

A strong synergistic shape-dependent photoactivity effect between platelet-like anatase TiO_2 morphology and surface fluorination is clearly outlined in RhB photodegradation, with an outstanding photoactivity increase observed only upon fluorination of the {001}-facet enriched material. This may result from an overall increased charge carriers separation combined with the higher amount of surface −OH groups in the platelet-like TiO_2 that can be fluorinated to generate F-{001} facets, which may considerably boost $^{\bullet}OH$ radical mediated oxidation paths.

The here unveiled role played by morphology and surface fluorination on the photoactivity of shape-controlled TiO_2 materials may pave the way for designing highly performant TiO_2-based materials to be employed in efficient photocatalytic detoxification processes.

Acknowledgements

The collaboration of Dr. Adele Scaltrini in performing photocatalytic oxidation/reduction kinetic runs and of Dr. Erica Montanari in carrying out HR-TEM measurements is gratefully acknowledged. This work received financial support from the University of Milano PSR2020_DIP_005_PI_MDOZZ project "Piano di Sostegno alla Ricerca 2020, linea 2, Azione A" and from the MIUR PRIN 20173397R7 MULTI-e project.

REFERENCES

[1] X. Zhou, N. Liu, P. Schmuki, Photocatalysis with TiO_2 Nanotubes: "Colorful" Reactivity and Designing Site-Specific Photocatalytic Centers into TiO_2 Nanotubes, ACS Catal. 7 (2017) 3210–3235. doi:10.1021/acscatal.6b03709.

[2] S. Wang, Z. Ding, X. Chang, J. Xu, D.-H. Wang, Modified Nano-TiO_2 Based Composites for Environmental Photocatalytic Applications, Catalysts. 10 (2020) 1–38.

[3] M. Gao, L. Zhu, W.L. Ong, J. Wang, G.W. Ho, Structural design of TiO_2-based photocatalyst for H_2 production and degradation applications, Catal. Sci. Technol. 5 (2015) 4703–4726. doi:10.1039/C5CY00879D.

[4] S.B. Patil, P.S. Basavarajappa, N. Ganganagappa, M.S. Jyothi, A.V. Raghu, K.R. Reddy, Recent advances in non-metals-doped TiO_2 nanostructured photocatalysts for visible-light driven hydrogen production, CO_2 reduction and air purification, Int. J. Hydrogen Energy. 44 (2019) 13022–13039. doi:10.1016/j.ijhydene.2019.03.164.

[5] A. Mittal, B. Mari, S. Sharma, V. Kumari, S. Maken, K. Kumari, N. Kumar, Non-metal modified TiO_2: a step towards visible light photocatalysis, J. Mater. Sci. Mater. Electron. 30 (2019) 3186–3207. doi:10.1007/s10854-018-00651-9.

[6] A. Truppi, F. Petronella, T. Placido, M. Striccoli, A. Agostiano, M. Curri, R. Comparelli, Visible-Light-Active TiO_2-Based Hybrid Nanocatalysts for Environmental Applications, Catalysts. 7 (2017) 100–1/33. doi:10.3390/catal7040100.

[7] S. Bera, D. Il Won, S.B. Rawal, H.J. Kang, W.I. Lee, Design of visible-light photocatalysts by coupling of inorganic semiconductors, Catal. Today. 335 (2019) 3–19. doi:10.1016/j.cattod.2018.11.001.

[8] H. Xu, S. Ouyang, L. Liu, P. Reunchan, N. Umezawa, J. Ye, Recent advances in TiO2-based photocatalysis, J. Mater. Chem. A. 2 (2014) 12642–12661. doi:10.1039/C4TA00941J.

[9] G. Li, K.A. Gray, The solid–solid interface: Explaining the high and unique photocatalytic reactivity of TiO_2-based nanocomposite materials, Chem. Phys. 339 (2007) 173–187. doi:10.1016/j.chemphys.2007.05.023.

[10] S.G. Kumar, K.S.R.K. Rao, Comparison of modification strategies towards enhanced charge carrier separation and photocatalytic degradation activity of metal oxide semiconductors (TiO_2, WO_3 and ZnO), Appl. Surf. Sci. 391 (2017) 124–148. doi:10.1016/j.apsusc.2016.07.081.

[11] Y. Li, L. Ding, Z. Liang, Y. Xue, H. Cui, J. Tian, Synergetic effect of defects rich MoS_2 and Ti_3C_2 MXene as cocatalysts for enhanced photocatalytic H_2 production activity of TiO_2, Chem. Eng. J. 383 (2020) 123178. doi:10.1016/j.cej.2019.123178.

[12] G. Liu, J.C. Yu, G.Q. (Max) Lu, H.-M. Cheng, Crystal facet engineering of semiconductor photocatalysts: motivations, advances and unique properties, Chem. Commun. 47 (2011) 6763–6783. doi:10.1039/c1cc10665a.

[13] W.-J. Ong, L.-L. Tan, S.-P. Chai, S.-T. Yong, A.R. Mohamed, Highly reactive {001} facets of TiO_2-based composites: synthesis, formation mechanism and characterization, Nanoscale. 6 (2014) 1946–2008. doi:10.1039/c3nr04655a.

[14] M.V. Dozzi, E. Selli, Specific Facets-Dominated Anatase TiO_2: Fluorine-Mediated Synthesis and Photoactivity, Catalysts. 3 (2013) 455–485. doi:10.3390/catal3020455.

[15] K. Wang, M. Janczarek, Z. Wei, T. Raja-Mogan, M. Endo-Kimura, T.M. Khedr, B.

Ohtani, E. Kowalska, Morphology-and crystalline composition-governed activity of titania-based photocatalysts: Overview and perspective, Catalysts. 9 (2019) 1054–1/30. doi:10.3390/catal9121054.

[16] M. Maisano, M.V. Dozzi, E. Selli, Searching for facet-dependent photoactivity of shape-controlled anatase TiO_2, J. Photochem. Photobiol. C Photochem. Rev. 28 (2016) 29–43. doi:10.1016/j.jphotochemrev.2016.07.002.

[17] Z. He, Q. Cai, M. Wu, Y. Shi, H. Fang, L. Li, J. Chen, J. Chen, S. Song, Photocatalytic Reduction of Cr(VI) in an Aqueous Suspension of Surface-Fluorinated Anatase TiO_2 Nanosheets with Exposed {001} Facets, Ind. Eng. Chem. Res. 52 (2013) 9556–9565. doi:10.1021/ie400812m.

[18] X. Li, J. Zhu, H. Li, Influence of crystal facets and F-modification on the photocatalytic performance of anatase TiO_2, Catal. Commun. 24 (2012) 20–24. doi:10.1016/j.catcom.2012.03.009.

[19] Z. He, L. Jiang, D. Wang, J. Qiu, J. Chen, S. Song, Simultaneous Oxidation of p-Chlorophenol and Reduction of Cr(VI) on Fluorinated Anatase TiO_2 Nanosheets with Dominant {001} Facets under Visible Irradiation, Ind. Eng. Chem. Res. 54 (2015) 808–818. doi:10.1021/ie503997m.

[20] H. Wu, J. Ma, Y. Li, C. Zhang, H. He, Photocatalytic oxidation of gaseous ammonia over fluorinated TiO_2 with exposed (001) facets, Appl. Catal. B Environ. 152–153 (2014) 82–87. doi:10.1016/j.apcatb.2014.01.021.

[21] P. Mikrut, M. Kobielusz, W. Macyk, Spectroelectrochemical characterization of euhedral anatase TiO_2 crystals – Implications for photoelectrochemical and photocatalytic properties of {001} {100} and {101} facets, Electrochim. Acta. 310 (2019) 256–265. doi:10.1016/j.electacta.2019.04.043.

[22] Q. Xiang, K. Lv, J. Yu, Pivotal role of fluorine in enhanced photocatalytic activity of anatase TiO_2 nanosheets with dominant (001) facets for the photocatalytic degradation of acetone in air, Appl. Catal. B Environ. 96 (2010) 557–564. doi:10.1016/j.apcatb.2010.03.020.

[23] K. Lv, Q. Xiang, J. Yu, Effect of calcination temperature on morphology and photocatalytic activity of anatase TiO_2 nanosheets with exposed {001} facets, Appl. Catal. B Environ. 104 (2011) 275–281. doi:10.1016/j.apcatb.2011.03.019.

[24] M. Maisano, M.V. Dozzi, M. Coduri, L. Artiglia, G. Granozzi, E. Selli, Unraveling the Multiple Effects Originating the Increased Oxidative Photoactivity of {001}-Facet Enriched Anatase TiO_2, ACS Appl. Mater. Interfaces. 8 (2016) 9745−9754. doi:10.1021/acsami.6b01808.

[25] M. Mrowetz, E. Selli, H_2O_2 evolution during the photocatalytic degradation of organic molecules on fluorinated TiO_2, New J. Chem. 30 (2006) 108–114. doi:10.1039/B511320B.

[26] M.V. Dozzi, E. Selli, Effects of phase composition and surface area on the photocatalytic paths on fluorinated titania, Catal. Today. 206 (2013) 26–31. doi:10.1016/j.cattod.2012.03.029.

[27] K. Lv, X. Li, K. Deng, J. Sun, X. Li, M. Li, Effect of phase structures on the photocatalytic activity of surface fluorinated TiO_2, Appl. Catal. B Environ. 95 (2010) 383–392. doi:10.1016/j.apcatb.2010.01.017.

[28] W. Choi, Pure and modified TiO_2 photocatalysts and their environmental applications, Catal. Surv. from Asia. 10 (2006) 16–28. doi:10.1007/s10563-006-9000-2.

[29] C. Minero, G. Mariella, V. Maurino, E. Pelizzetti, Photocatalytic Transformation of Organic Compounds in the Presence of Inorganic Anions. 1. Hydroxyl-Mediated and Direct Electron-Transfer Reactions of Phenol on a Titanium Dioxide−Fluoride System, Langmuir. 16 (2000) 2632–2641. doi:10.1021/la9903301.

[30] J. Kim, W. Choi, H. Park, Effects of TiO_2 surface fluorination on photocatalytic degradation of methylene blue and humic acid, Res. Chem. Intermed. 36 (2010) 127–140. doi:10.1007/s11164-010-0123-8.

[31] Y. Ku, I.-L. Jung, Photocatalytic reduction of Cr(VI) in aqueous solutions by UV irradiation with the presence of titanium dioxide, Water Res. 35 (2001) 135–142. doi:10.1016/S0043-1354(00)00098-1.

[32] P. Qu, J. Zhao, T. Shen, H. Hidaka, TiO_2-assisted photodegradation of dyes: A study of two competitive primary processes in the degradation of RB in an aqueous TiO_2 colloidal solution, J. Mol. Catal. A Chem. 129 (1998) 257–268. doi:10.1016/S1381-1169(97)00185-4.

[33] L. Qi, J. Yu, M. Jaroniec, Enhanced and suppressed effects of ionic liquid on the photocatalytic activity of TiO_2, Adsorption. 19 (2013) 557–561. doi:10.1007/s10450-013-9478-7.

[34] J. Ke, M. Adnan Younis, Y. Kong, H. Zhou, J. Liu, L. Lei, Y. Hou, Nanostructured Ternary Metal Tungstate-Based Photocatalysts for Environmental Purification and Solar Water Splitting: A Review, Nano-Micro Lett. 10 (2018) 1–27. doi:10.1007/s40820-018-0222-4.

[35] H. Park, Y. Park, W. Kim, W. Choi, Surface modification of TiO_2 photocatalyst for environmental applications, J. Photochem. Photobiol. C Photochem. Rev. 15 (2013) 1–20. doi:10.1016/j.jphotochemrev.2012.10.001.

[36] Y.H. Chiu, T.F.M. Chang, C.Y. Chen, M. Sone, Y.J. Hsu, Mechanistic insights into photodegradation of organic dyes using heterostructure photocatalysts, Catalysts. 9 (2019) 430–1/32. doi:10.3390/catal9050430.

[37] M.V. Dozzi, A. Saccomanni, E. Selli, Cr(VI) photocatalytic reduction: Effects of simultaneous organics oxidation and of gold nanoparticles photodeposition on TiO_2, J. Hazard. Mater. 211 (2012) 188–195. doi:10.1016/j.jhazmat.2011.09.038.

[38] Y.-X. Li, X. Wang, C.-C. Wang, H. Fu, Y. Liu, P. Wang, C. Zhao, S-TiO_2/UiO-66-NH_2 composite for boosted photocatalytic Cr(VI) reduction and bisphenol A degradation under LED visible light, J. Hazard. Mater. 399 (2020) 123085–1/14. doi:10.1016/j.jhazmat.2020.123085.

[39] Y.X. Li, H. Fu, P. Wang, C. Zhao, W. Liu, C.C. Wang, Porous tube-like ZnS derived from rod-like ZIF-L for photocatalytic Cr(VI) reduction and organic pollutants degradation, Environ. Pollut. 256 (2020) 113417–1/13. doi:10.1016/j.envpol.2019.113417.

[40] C.D. Palmer, P.R. Wittbrodt, Processes affecting the remediation of chromium-contaminated sites., Environ. Health Perspect. 92 (1991) 25–40. doi:10.1289/ehp.919225.

[41] V. Bianchi, A. Zantedeschi, A. Montaldi, F. Majone, Trivalent chromium is neither

cytotoxic nor mutagenic in permeabilized hamster fibroblasts, Toxicol. Lett. 23 (1984) 51–59. doi:10.1016/0378-4274(84)90009-2.

[42] Y.Y. Cheng, T.H. Tsai, Pharmacokinetics and Biodistribution of the Illegal Food Colorant Rhodamine B in Rats, J. Agric. Food Chem. 65 (2017) 1078–1085. doi:10.1021/acs.jafc.6b04975.

[43] L. Spessato, V.A. Duarte, P. Viero, H. Zanella, J.M. Fonseca, P.A. Arroyo, V.C. Almeida, Optimization of Sibipiruna activated carbon preparation by simplex-centroid mixture design for simultaneous adsorption of rhodamine B and metformin, J. Hazard. Mater. 411 (2021) 125166–1/16. doi:10.1016/j.jhazmat.2021.125166.

[44] J.S. Chen, X.W. Lou, Anatase TiO_2 nanosheet: An ideal host structure for fast and efficient lithium insertion/extraction, Electrochem. Commun. 11 (2009) 2332–2335. doi:10.1016/j.elecom.2009.10.024.

[45] H. Wu, J. Ma, Y. Li, C. Zhang, H. He, Photocatalytic oxidation of gaseous ammonia over fluorinated TiO_2 with exposed (001) facets, Appl. Catal. B Environ. 152–153 (2014) 82–87. doi:10.1016/j.apcatb.2014.01.021.

[46] M. Coduri, M. Maisano, M.V. Dozzi, E. Selli, Morphological characterization of shape-controlled TiO_2 anatase through XRPD analysis, Zeitschrift Fur Phys. Chemie. 230 (2016) 1233–1248. doi:10.1515/zpch-2015-0715.

[47] B.H. Toby, R.B. Von Dreele, GSAS-II: The genesis of a modern open-source all purpose crystallography software package, J. Appl. Crystallogr. 46 (2013) 544–549. doi:10.1107/S0021889813003531.

[48] M.V. Dozzi, L. Prati, P. Canton, E. Selli, Effects of gold nanoparticles deposition on the photocatalytic activity of titanium dioxide under visible light., Phys. Chem. Chem. Phys. 11 (2009) 7171–7180.

[49] M. Abdullah, G.K.C. Low, R.W. Matthews, Effects of common inorganic anions on rates of photocatalytic oxidation of organic carbon over illuminated titanium dioxide, J. Phys. Chem. 94 (1990) 6820–6825. doi:10.1021/j100380a051.

[50] X. Wang, S.O. Pehkonen, A.K. Ray, Removal of Aqueous Cr(VI) by a Combination of Photocatalytic Reduction and Coprecipitation, Ind. Eng. Chem. Res. 43 (2004) 1665–1672. doi:10.1021/ie030580j.

[51] L.S. Clesceri, A.E. Greenberg, A.D. Eaton, Standard Methods for the Examination of Water and Wastewater, 20th Ed., 1998.

[52] C. Bernardini, G. Cappelletti, M.V. Dozzi, E. Selli, Photocatalytic degradation of organic molecules in water: Photoactivity and reaction paths in relation to TiO_2 particles features, J. Photochem. Photobiol. A Chem. 211 (2010) 185–192. doi:10.1016/j.jphotochem.2010.03.006.

[53] H.M. Rietveld, A profile refinement method for nuclear and magnetic structures, J. Appl. Crystallogr. 2 (1969) 65–71. doi:10.1107/S0021889869006558.

[54] L. Mino, F. Pellegrino, S. Rades, J. Radnik, V.D. Hodoroaba, G. Spoto, V. Maurino, G. Martra, Beyond Shape Engineering of TiO_2 Nanoparticles: Post-Synthesis Treatment Dependence of Surface Hydration, Hydroxylation, Lewis Acidity and Photocatalytic Activity of TiO_2 Anatase Nanoparticles with Dominant {001} or {101} Facets, ACS Appl. Nano Mater. 1 (2018) 5355–5365. doi:10.1021/acsanm.8b01477.

[55] L. Ye, J. Mao, J. Liu, Z. Jiang, T. Peng, L. Zan, Synthesis of anatase TiO_2 nanocrystals

with {101}, {001} or {010} single facets of 90% level exposure and liquid-phase photocatalytic reduction and oxidation activity orders, J. Mater. Chem. A. 1 (2013) 10532–10537. doi:10.1039/c3ta11791j.

[56] L. Liu, Z. Liu, A. Liu, X. Gu, C. Ge, F. Gao, L. Dong, Engineering the TiO_2-graphene interface to enhance photocatalytic H_2 production, ChemSusChem. 7 (2014) 618–626. doi:10.1002/cssc.201300941.

[57] T. Li, B. Tian, J. Zhang, R. Dong, T. Wang, F. Yang, Facile tailoring of anatase TiO_2 morphology by use of H_2O_2: From microflowers with dominant {101} facets to microspheres with exposed {001} facets, Ind. Eng. Chem. Res. 52 (2013) 6704–6712. doi:10.1021/ie3030714.

[58] Y. Luan, L. Jing, Y. Xie, X. Sun, Y. Feng, H. Fu, Exceptional photocatalytic activity of 001-facet-exposed TiO_2 mainly depending on enhanced adsorbed oxygen by residual hydrogen fluoride, ACS Catal. 3 (2013) 1378–1385. doi:10.1021/cs400216a.

[59] C. Li, C. Koenigsmann, W. Ding, B. Rudshteyn, K.R. Yang, K.P. Regan, S.J. Konezny, V.S. Batista, G.W. Brudvig, C.A. Schmuttenmaer, J.-H. Kim, Facet-Dependent Photoelectrochemical Performance of TiO_2 Nanostructures: An Experimental and Computational Study, J. Am. Chem. Soc. 137 (2015) 1520–1529. doi:10.1021/ja5111078.

[60] J. Yu, J. Low, W. Xiao, P. Zhou, M. Jaroniec, Enhanced Photocatalytic CO_2-Reduction Activity of Anatase TiO_2 by Coexposed {001} and {101} Facets, J. Am. Chem. Soc. 136 (2014) 8839–8842. doi:10.1021/ja5044787.

[61] M. Bernareggi, M.V. Dozzi, L. Bettini, A. Ferretti, G. Chiarello, E. Selli, Flame-Made Cu/TiO_2 and $Cu\text{-}Pt/TiO_2$ Photocatalysts for Hydrogen Production, Catalysts. 7 (2017) 301–1/14. doi:10.3390/catal7100301.

[62] G. Wu, J. Wang, D.F. Thomas, A. Chen, Synthesis of F-Doped Flower-like TiO_2 Nanostructures with High Photoelectrochemical Activity, Langmuir. 24 (2008) 3503–3509. doi:10.1021/la703098g.

[63] J.C. Yu, J. Yu, H. Wingkei, J. Zitao, Z. Lizhi, Effects of F^- Doping on the Photocatalytic Activity and Microstructures of Nanocrystalline TiO_2 Powders, Chem. Mater. 14 (2002) 3808–3816. doi:10.1021/cm020027c.

[64] M.V. Dozzi, L. Artiglia, G. Granozzi, B. Ohtani, E. Selli, Photocatalytic Activity vs Structural Features of Titanium Dioxide Materials Singly Doped or Codoped with Fluorine and Boron, J. Phys. Chem. C. 118 (2014) 25579−25589.

[65] C.H. Weng, J.H. Wang, C.P. Huang, Adsorption of Cr(VI) onto TiO_2 from dilute aqueous solutions, Water Sci. Technol. 35 (1997) 55–62.

[66] M. Kosmulski, The significance of the difference in the point of zero charge between rutile and anatase, Adv. Colloid Interface Sci. 99 (2002) 255–264. doi:10.1016/S0001-8686(02)00080-5.

[67] S. Asuha, X.G. Zhou, S. Zhao, Adsorption of methyl orange and Cr(VI) on mesoporous TiO_2 prepared by hydrothermal method, J. Hazard. Mater. 181 (2010) 204–210. doi:10.1016/j.jhazmat.2010.04.117.

[68] N. Fessi, M.F. Nsib, L. Cardenas, C. Guillard, F. Dappozze, A. Houas, F. Parrino, L. Palmisano, G. Ledoux, D. Amans, Y. Chevalier, Surface and Electronic Features of Fluorinated TiO_2 and Their Influence on the Photocatalytic Degradation of 1-

Methylnaphthalene, J. Phys. Chem. C. 124 (2020) 11456–11468. doi:10.1021/acs.jpcc.0c01929.

[69] H. Park, W. Choi, Effects of TiO_2 Surface Fluorination on Photocatalytic Reactions and Photoelectrochemical Behaviors, J. Phys. Chem. B. 108 (2004) 4086–4093. doi:10.1021/jp036735i.

[70] G. Di Liberto, S. Tosoni, G. Pacchioni, Role of Heterojunction in Charge Carrier Separation in Coexposed Anatase (001)-(101) Surfaces, J. Phys. Chem. Lett. 10 (2019) 2372–2377. doi:10.1021/acs.jpclett.9b00504.

[71] T. Ohno, K. Sarukawa, M. Matsumura, Crystal faces of rutile and anatase TiO_2 particles and their roles in photocatalytic reactions, New J. Chem. 26 (2002) 1167–1170. doi:10.1039/b202140d.

[72] Z. Zheng, B. Huang, J. Lu, X. Qin, X. Zhang, Y. Dai, Hierarchical TiO_2 Microspheres: Synergetic Effect of {001} and {101} Facets for Enhanced Photocatalytic Activity, Chem. - A Eur. J. 17 (2011) 15032–15038. doi:10.1002/chem.201101466.

[73] F. Pellegrino, F. Sordello, L. Mino, C. Minero, V.D. Hodoroaba, G. Martra, V. Maurino, Formic Acid Photoreforming for Hydrogen Production on Shape-Controlled Anatase TiO_2 Nanoparticles: Assessment of the Role of Fluorides, {101}/{001} Surfaces Ratio, and Platinization, ACS Catal. 9 (2019) 6692–6697. doi:10.1021/acscatal.9b01861.

[74] P. Deák, B. Aradi, T. Frauenheim, Band Lineup and Charge Carrier Separation in Mixed Rutile-Anatase Systems, J. Phys. Chem. C. 115 (2011) 3443–3446. doi:10.1021/jp1115492.

[75] M. Lazzeri, A. Vittadini, A. Selloni, Structure and energetics of stoichiometric TiO_2 anatase surfaces, 63 (2001) 1–9. doi:10.1103/PhysRevB.63.155409.

[76] P. Zhou, H. Zhang, H. Ji, W. Ma, C. Chen, J. Zhao, Modulating the photocatalytic redox preferences between anatase TiO_2 {001} and {101} surfaces, Chem. Commun. 53 (2017) 787–790. doi:10.1039/C6CC08785J.

[77] C. Arrouvel, M. Digne, M. Breysse, H. Toulhoat, P. Raybaud, Effects of morphology on surface hydroxyl concentration: A DFT comparison of anatase-TiO_2 and γ-alumina catalytic supports, J. Catal. 222 (2004) 152–166. doi:10.1016/j.jcat.2003.10.016.

[78] L. Mino, Á. Morales-García, S.T. Bromley, F. Illas, Understanding the nature and location of hydroxyl groups on hydrated titania nanoparticles, Nanoscale. 13 (2021) 6577–6585. doi:10.1039/d1nr00610j.

[79] M. Mrowetz, E. Selli, H_2O_2 evolution during the photocatalytic degradation of organic molecules on fluorinated TiO_2, New J. Chem. 30 (2006) 108–114. doi:10.1039/b511320b.

[80] Q. Wang, C. Chen, D. Zhao, M. Wanhong, J. Zhao, Change of adsorption modes of dyes on fluorinated TiO_2 and its effect on photocatalytic degradation of dyes under visible irradiation, Langmuir. 24 (2008) 7338–7345. doi:10.1021/la800313s.

[81] C. Yao, X. Wang, W. Zhao, T. Li, Y. He, X. Ran, L. Guo, Probing the facet-dependent intermediate in the visible-light degradation of RhB by carbon-coated anatase TiO_2 nanoparticles, J. Alloys Compd. 846 (2020) 156335–1/9. doi:10.1016/j.jallcom.2020.156335.

[82] Y. Hu, D. Li, H. Wang, G. Zeng, X. Li, Y. Shao, Role of active oxygen species in the liquid-phase photocatalytic degradation of RhB using $BiVO_4$/TiO_2 heterostructure under

visible light irradiation, J. Mol. Catal. A Chem. 408 (2015) 172–178. doi:10.1016/j.molcata.2015.07.025.

[83] M. Mrowetz, E. Selli, Enhanced photocatalytic formation of hydroxyl radicals on fluorinated TiO_2, Phys. Chem. Chem. Phys. 7 (2005) 1100–1102. doi:10.1039/b500194c.

[84] M. Chen, J. Ma, B. Zhang, G. He, Y. Li, C. Zhang, H. He, Remarkable synergistic effect between {001} facets and surface F ions promoting hole migration on anatase TiO_2, Appl. Catal. B Environ. 207 (2017) 397–403. doi:10.1016/j.apcatb.2017.02.048.

[85] H. Sheng, Q. Li, W. Ma, H. Ji, C. Chen, J. Zhao, Photocatalytic degradation of organic pollutants on surface anionized TiO_2: Common effect of anions for high hole-availability by water, Appl. Catal. B Environ. 138–139 (2013) 212–218. doi:10.1016/j.apcatb.2013.03.001.

[86] L. Mino, C. Negri, R. Santalucia, G. Cerrato, G. Spoto, G. Martra, Morphology , Surface Structure and Water Adsorption Properties of TiO_2 Nanoparticles: A Comparison of Different Commercial Samples, Molecules. 25 (2020) 4605.

[87] A. Mahdavi-Shakib, J.M. Arce-Ramos, R.N. Austin, T.J. Schwartz, L.C. Grabow, B.G. Frederick, Frequencies and Thermal Stability of Isolated Surface Hydroxyls on Pyrogenic TiO_2 Nanoparticles, J. Phys. Chem. C. 123 (2019) 24533–24548. doi:10.1021/acs.jpcc.9b05699.

[88] C. Sun, L.M. Liu, A. Selloni, G.Q. Lu, S.C. Smith, Titania-water interactions: A review of theoretical studies, J. Mater. Chem. 20 (2010) 10319–10334. doi:10.1039/c0jm01491e.